2025 IEEE 64th Conference on Decision and Control (CDC)
December 10-12, 2025. Rio de Janeiro, Brazil

A Causal Approach to Hard Constrained Control of Wave Energy Systems based on an Implicit Gaussian Differential Equation

Jorge L. Anderson-Azzano[1], Pedro Fornaro[2,1], Paul F. Puleston[1] and John V. Ringwood[2]

***Abstract*— This paper introduces a novel method to causally satisfy hard position *and* velocity constraints in wave energy systems. The constraint mechanism is simple to implement, computationally efficient, and does not require complex tuning or optimisation techniques. The proposed strategy handles system constraints by modulating a velocity reference with a Gaussian-like envelope function that depends on both position and velocity, which results in nonlinear closed-loop dynamics. In this context, this paper focuses on the stability of the constrained closed-loop dynamics, and it is proven that, for a set of initial conditions within the constraint region, the system trajectories remain within the prescribed limits. Finally, in-silico evaluations demonstrate that the Gaussian-like function effectively guarantees compliance with system constraints and is broadly applicable to wave energy systems.**

I. Introduction

Wave energy control strategies may be broadly divided into two categories: Optimisation-based (OB) and non-OB (!OB) strategies [1]. OB control provides constrained energy-maximizing solutions by resorting to numerical routines. However, the effectiveness of OB controllers depends on the WEC model precision and robust OB control exhibits marginal advantage in terms of energy absorption [1]. Additionally, for solutions close to the constraint limits, OB methods can become computationally intractable and, in practice, not implementable [2][3].

In contrast, !OB control strategies do not rely on numerical routines and provide (suboptimal) real-time implementable solutions [4]. Although !OB strategies represent an attractive alternative to implementing real-time control of wave energy converters (WECs), none of the existing !OB strategies can efficiently handle position *and* velocity constraints, as thoroughly detailed in [4]. It is worth noting that add-on techniques (as in [5][6][7]) could be used to handle (only) position constraints.

Symphony, a recently emerged !OB controller [8], presents a novel method to handle both position *and* velocity constraints. The advantages of the proposed constraint method include a low computational burden, simplicity of use and implementation, and, fundamentally, independence of the WEC model with close-to-optimal performance in terms of power absorption (see [8]). However, the method is based on modulating a velocity reference with a Gaussian envelope function, which results in nonlinear closed-loop dynamics. Specifically, the position dynamics are governed by an Implicit Gaussian Differential Equation (IGDE). In this context, the goal of this paper is to assess the closed-loop stability of the resultant IGDE of Symphony, which proves essential for the application of the constraint mechanism.

In order to solve the IGDE stability problem, first, it is proven that, for a set of initial conditions inside the constraints region, $\mathcal{R}_c$, the system trajectories remain inside $\mathcal{R}_c$. Second, assuming the excitation force belongs to a class of periodic functions with zero mean, the existence and stability of a limit cycle is numerically evaluated via Poincaré maps. Importantly, although the panchromatic case is not formally analysed in this paper, an extrapolation of the results could be made by resorting to, for instance, [9].

The remainder of this paper is organised as follows. First, the problem formulation is presented in Section II. In Section III the stability analysis is conducted. Then, a numerical example based on WECs is presented in Section IV. Finally, conclusions are drawn in Section V.

II. Problem formulation

Consider the normalized one-degree-of-freedom WEC dynamics under external excitation:

$$\Sigma_w : \begin{cases} \dot{z} = v, & \text{(1a)} \\ \dot{v} = -z - v - \mathbf{h}\boldsymbol{q} + f_u + f_e, & \text{(1b)} \\ \dot{\boldsymbol{q}} = \mathbf{F}\boldsymbol{q} + \mathbf{g}v, & \text{(1c)} \end{cases}$$

where $z \in \mathbb{R}$ is the body position, $v \in \mathbb{R}$ is the velocity, $\boldsymbol{q} \in \mathbb{R}^r$ are the radiation states, with the triple $(\mathbf{F}, \mathbf{g}, \mathbf{h})$ being passive [10], $f_e : \mathbb{R} \to \mathbb{R}$ is a normalized external force with zero mean value and $f_u : \mathbb{R} \to \mathbb{R}$ is the control force. Additionally, assume system (1) is subject to position and velocity constraints:

$$|z|/z_M < 1 \quad \text{and} \quad |v|/v_M < 1, \tag{2}$$

with z_M, $v_M \in \mathbb{R}_+$. In a vast majority of the existing literature, the WEC control problem is associated with maximising a cost function over a time interval $T \in \mathbb{R}_+$, subject to system constraints as [11]:

$$\begin{aligned} f_u = \arg\max_{f_u} &\{\mathcal{J}_T(f_u)\}, \\ &\text{s.t.} \\ &\text{System dynamics (1)}, \\ &\text{Constraints (2)}, \end{aligned} \tag{3}$$

where f_u is designed to maximise the cost function $\mathcal{J}_T(f_u)$, typically associated with useful energy. Typically, to solve

This research has been conducted with the financial support of Taighde Éireann – Research Ireland under grant number 21/US/3776, and of the University Nacional de La Plata, CONICET and ANCyT, Argentina.

[1] GECEP-Instituto LEICI, Facultad de Ingeniería/UNLP - CONICET, La Plata, Bs.As., Argentina.

[2] Centre for Ocean Energy Research, Department of Electronic Engineering, Maynooth University, Co. Kildare, Ireland.

problem (3), !OB controllers provide an unconstrained reference $\bar{v}$, which is then suboptimally altered to comply with system constraints using auxiliary mechanisms. The constraint mechanism analysed in this paper (preliminarily presented in Symphony) operates by modulating $\bar{v} := k_0 \cdot \hat{f}_e$, (with $\hat{f}_e$ being an estimation of the excitation force and $k_0 \in \mathbb{R}_+$ a design parameter) with a Gaussian-like envelope. Specifically, assuming system (1) is controlled with a sufficiently robust tracking controller, the modulated velocity reference, v^*, is defined as:

$$v^* \equiv \dot{z} = \underbrace{\left(\frac{e^{1-\alpha(z,\dot{z})}-1}{e^1-1}\right) \cdot k_0 \ \hat{f}_e}_{F(\hat{f}_e,z,\dot{z})} = g(z,\dot{z}) \cdot k_0 \ \hat{f}_e, \quad (4)$$

with:

$$\alpha(z,\dot{z}) = z^2 + \dot{z}^2 + z\dot{z}. \quad (5)$$

Notably, the modulating envelope $g(z,\dot{z})$, in (4), can be employed with any !OB control that provides $\bar{v}$. In the following, $\hat{f}_e := f_e$, $v_M = z_M = 1$, and $k_0 = 1$ are assumed, since neither variable affects the IGDE stability analysis.

The main goal of this paper is to prove that v^*, in (4), can be used as a velocity reference to satisfy constraints (2) $\forall t$ robustly. Specifically, considering the standing assumptions:

(H1) $f_e(t)$ is a *smooth* bounded function of time, with $|f_e(t)| \leqslant A < \infty$,
(H2) $f_e(t)$ is a periodic function with zero mean,
(H3) Any given set of initial conditions $\boldsymbol{z}_0 = [z_0 \ \dot{z}_0] \in \mathbb{R}^2$ satisfies $\alpha(z_0,\dot{z}_0) < 1$,

it is proven that the ellipse equation defined by:

$$\alpha(z,\dot{z}) = 1, \quad (6)$$

acts as a boundary surface for the operational space of the WEC position and velocity, i.e., a limit region that both z and $\dot{z}$ cannot surpass.

III. Stability study of the Nonlinear IGDE

In this section, the stability analysis for IGDE (4) is conducted considering (H1)–(H3). First, a preliminary analysis is conducted in Subsection III-A. In Subsection III-B, it is established that both position and velocity remain within an invariance region enclosed by (6), ensuring compliance with the system constraints. Next, in Subsection III-C, it is proved, through Poincaré map analysis, that under a periodic f_e, the system exhibits bounded periodic oscillations.

A. Preliminary analysis

This section presents a preliminary conceptual analysis of (4). First, note that $g(z,\dot{z}) > 0$, $\forall \boldsymbol{z} \in \mathcal{R}_z = \{\boldsymbol{z} \in \mathbb{R}^2 : \alpha(z,\dot{z}) < 1\}$, where $\boldsymbol{z} = [z \ \dot{z}]^\intercal$. Also, due to the algebraic dependency between f_e, z, and $\dot{z}$ in (4), the possible system trajectories and initial conditions are limited. For instance, for a given f_e and z, the velocity $\dot{z}$ is unequivocally determined.

Importantly, note that as $\alpha(z,\dot{z}) \to 1$, $g(z,\dot{z}) \to 0$, diminishing v^*. Hence, it is expected that every possible trajectory is limited by the ellipse (6). In fact, it is possible to conduct a preliminary limit evaluation using:

$$\frac{1}{\sqrt{2}} \ f_e(t) = \frac{1}{\sqrt{2}} \frac{\dot{z}}{g(z,\dot{z})} := V^{1/2}(z,\dot{z}), \quad (7)$$

and taking the limit:

$$\lim_{\alpha(z,\dot{z})\to 1} V^{1/2}(z,\dot{z}) \to \infty. \quad (8)$$

Thus, only with a force tending to infinity the system trajectories reach the ellipse limits. Two important points in the plane are: $z = \pm 1$, for which $\dot{z} = 0 \ \forall t$ and all $f_e(t)$. Hence, it is also essential to prove that no trajectory ends in $z = \pm 1$. Thus, the following analysis focuses on evaluating system trajectories inside ellipse (6) and the existence of a periodic oscillatory evolution of z, thereby guaranteeing $|z| < 1, \ \forall t$.

B. Invariance region for system position and velocity

In this section, it is proven that, considering (H1) and (H3), the differential equation (4) defines a region that contains all possible trajectories for both, position z and velocity $\dot{z}$ of system (1).

In order to compute the system trajectories $\boldsymbol{z}(t)$, obtain the velocity dynamics as follows:

$$\ddot{z} = \frac{\partial F}{\partial z}\dot{z} + \frac{\partial F}{\partial \dot{z}}\ddot{z} + \frac{\partial F}{\partial f_e}\dot{f}_e, \quad (9)$$

which leads to the explicit differential equation:

$$\ddot{z} = \frac{\frac{\partial F}{\partial z}}{1-\frac{\partial F}{\partial \dot{z}}}\dot{z} + \frac{\frac{\partial F}{\partial f_e}}{1-\frac{\partial F}{\partial \dot{z}}}\dot{f}_e. \quad (10)$$

Observe that the partial derivatives of $\frac{\partial F}{\partial z}$ and $\frac{\partial F}{\partial \dot{z}}$ are nonlinear functions in the state z, its first derivative $\dot{z}$ and the external force f_e. Now, to evaluate the evolution of the system trajectories, use the positive semidefinite function:

$$\frac{1}{2} \ f_e^2(t) = \frac{1}{2}\left(\frac{\dot{z}}{g(\boldsymbol{z})}\right)^2 := V(\boldsymbol{z}). \quad (11)$$

Note that V is well-defined for all values of $\boldsymbol{z} \in \mathcal{R}_z$, since $g(\boldsymbol{z}) > 0$, $\forall \boldsymbol{z} \in \mathcal{R}_z$. Let $f_e = A \in \mathbb{R}\backslash\{0\}$ and define a level curve of (11) as:

$$\mathcal{S}_V = \left\{\boldsymbol{z} \in \mathcal{R}_z : V(\boldsymbol{z}) = 0.5A^2\right\}. \quad (12)$$

Then, for any $f_e(t)$ satisfying (H1), define the constrained region $\mathcal{R}_c$ as:

$$\mathcal{R}_c = \left\{\boldsymbol{z} \in \mathcal{R}_z : V(\boldsymbol{z}) \leqslant 0.5A^2\right\}. \quad (13)$$

A graphical representation of the function V and the level curve $\mathcal{S}_V$ is shown in Figure 1.

Now, assuming (H1) holds, it is proven that the trajectories of system (4) become tangential to $\mathcal{S}_V$ as they approach to it and, hence, they cannot surpass $\mathcal{S}_V$. Equivalently, the trajectories are normal to the gradient of V:

$$\nabla V(\boldsymbol{z}) = \begin{bmatrix} -2\dfrac{V(\boldsymbol{z})}{g(\boldsymbol{z})}\dfrac{\partial g(\boldsymbol{z})}{\partial z} \\ 2V(\boldsymbol{z})\left(\dfrac{1}{\dot{z}} - \dfrac{1}{g(\boldsymbol{z})}\dfrac{\delta g(\boldsymbol{z})}{\partial \dot{z}}\right) \end{bmatrix}^\intercal. \quad (14)$$

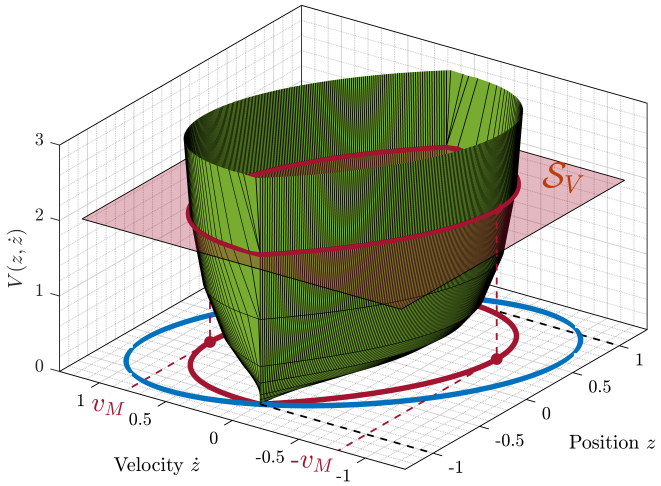

Figure 1. Graphical representation of function V with its level curve $\mathcal{S}_V$.

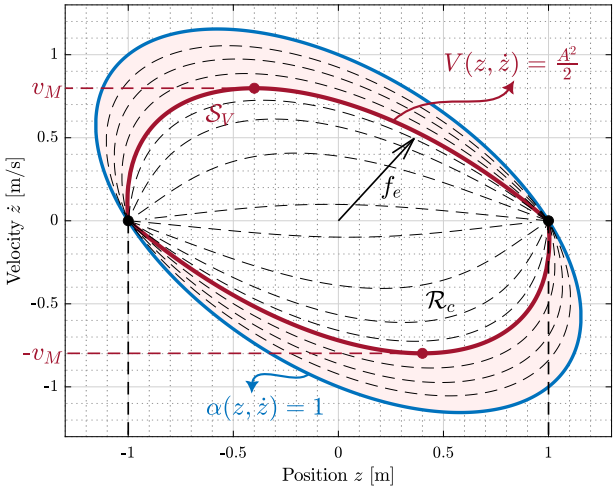

Figure 2. Space constraints for the system variables, z vs. $\dot{z}$.

By computing the internal product, using system dynamic (10) and (H1), it follows that $\lim_{f_e \to A} \dot{f}_e = 0$ and, thus:

$$\nabla V \cdot \left[\begin{matrix}\dot{z}\\ \ddot{z}\end{matrix}\right]\Bigg|_{\mathcal{S}_V} = -A^2 \left(A\frac{\partial g}{\partial z} - \frac{\left(1 - A\partial\frac{\partial g}{\partial \dot{z}}\right) f_e \frac{\partial g}{\partial z}}{1 - f_e \frac{\partial g}{\partial \dot{z}}} \right), \quad (15)$$

where it can be easily shown that:

$$\lim_{f_e \to A} \nabla V \cdot \left[\begin{matrix}\dot{z}\\ \ddot{z}\end{matrix}\right]\Bigg|_{\mathcal{S}_V} = 0, \quad (16)$$

which proves invariance of $\mathcal{R}_c$, in accordance with Nagumo's theorem. That is, for an external force satisfying (H1), any trajectory starting inside $\mathcal{R}_c$ remains in $\mathcal{R}_c$, $\forall t$.

Now, let $\dot{f}_e = 0$ with some finite $f_e \in \mathbb{R}\backslash\{0\}$, then the resultant phase diagrams for different f_e values are illustrated in Figure 2. Here, each dashed line represents a system restriction for a given fixed value of f_e. Consequently, the system trajectories are tangential to the level curves (dashed lines) when $\dot{f}_e$ vanishes. Also, note that the outer ellipse (solid blue line) is the major curve defined by (6), which is obtained with $f_e \to \infty$ and, hence, it defines the region from which the system trajectories cannot escape.

Two important remarks are in order. First, note that, due to the orthogonality between z and $\dot{z}$, when $\dot{z} = 0$, $\forall z \in (-1, 1)$, the system trajectories are perpendicular to the z axis. So, z is absolutely bounded by 1, since there are no trajectories crossing the z axis for $|z| > 1$. Second, for a given $f_e(t)$ satisfying (H1), $\mathcal{R}_c$ defines a bound for the system velocity $\dot{z}$, given by v_M:

$$v_M = \max\{|\dot{z}|\}, \quad \forall \dot{z} \in \mathcal{S}_V. \quad (17)$$

An illustrative example for $f_e = A = 2$ is presented in Figure 2.

C. Existence of forced oscillations

The previous analysis defines the existence of an invariance region from which the system trajectories cannot escape. Now, the study is extended to prove that, considering (H2), the system trajectories inside $\mathcal{R}_c$ exhibit a forced oscillation. To that end, Poincaré maps are used. A Poincaré map provides a *snap-shot* of all trajectories crossing through a specific region in the state-space, namely a Poincaré section. Hence, by appropriate selection of a Poincaré section, it is possible to prove existence and stability of periodic orbits in system trajectories.

Formally, let $z(t)$ be a solution of (4), with $z(t_0) = z_0$. Then a Poincaré map, P, maps z_0 into $z(T)$, i.e., $z(T) = P(z_0)$. Hence, the problem of finding stable oscillations is reduced to that of finding a fixed point for the map P [9].

To conduct a Poincaré analysis, it is assumed that the excitation force is of the form:

$$f_e(t) = A(t) \sin\left(\int_{t_0}^{t} \omega(\tau)\delta\tau \right), \quad (18)$$

where $A(t)$ and $\omega(t)$ are slowly varying parameters, dependent on the sea spectrum characteristics [12]. First, Poincaré maps are built for monochromatic cases, assuming constant amplitudes A and frequencies ω. Hence, (4) can be reformulated as an autonomous system, as follows:

$$\begin{aligned} \dot{z} &= A\sin(\theta) \cdot g(\boldsymbol{z}), \\ \dot{\theta} &= \omega. \end{aligned} \quad (19)$$

As seen in (19), the modulation function g does not contribute to the system phase, meaning that the velocity zero crossings always coincide with those of f_e. The synchronisation between $\dot{z}$ and f_e is used to construct a Poincaré map, capturing the system state at the plane defined by $\theta = (2n+1)\pi$, with $n \in \mathbb{Z}$. Thus, the Poincaré section is defined as:

$$\mathcal{S}_P = \{(z, \theta) \in \mathbb{R}^2 : \theta = (2k+1)\pi, \forall k \in \mathbb{Z}\}, \quad (20)$$

which is crossed by all system trajectories in $\mathcal{R}_c$. Then, the existence and stability of a periodic solution are evaluated using the discrete recurrence relation:

$$z_{n+1} = P(z_n), \quad (21)$$

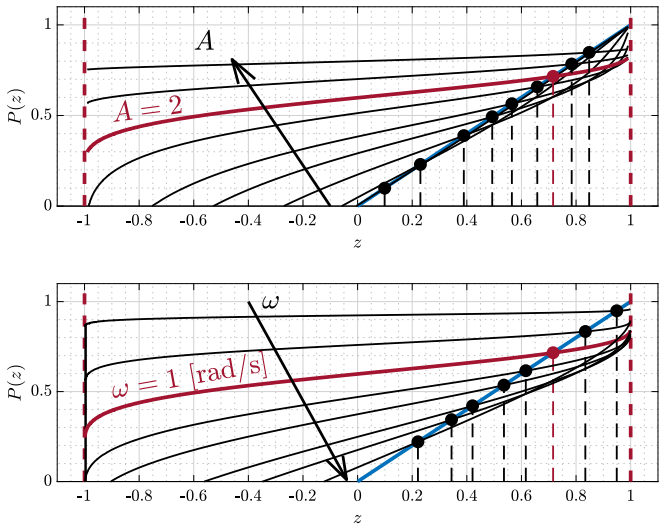

Figure 3. Poincaré maps, $P(z)$, of system trajectories for different force amplitudes (top) and frequencies (bottom).

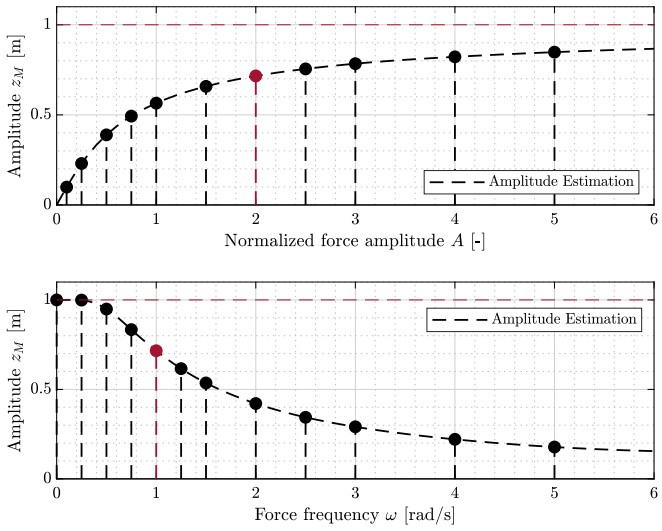

Figure 4. Maximum displacement of position z, z_M, as a function of force amplitude (top) and frequency (bottom).

where $P(z)$ is the Poincaré map of the system. In words, P provides the values of z that recurrently go through the Poincaré section (20) and, then, the main goal consists of finding fixed points, where $z^*_{n+1} = z^*_n$. Notably, choosing the Poincaré surface as in (20), the fixed points of P, denoted as z^*_n, determine the maximum displacement of z in stationary condition.

Due to the implicit form of (4), it is not possible to find an analytic solution for $z(t)$ and, hence, the Poincaré maps are computed numerically. Figure 3 presents $P(z)$ (solid black curves) for different amplitudes A and frequencies ω. Additionally, the solid red curve in represents a nominal condition for the external force, i.e., $A = A_n = 2$ and $\omega = \omega_n = 1$ [rad/s]. The intersection of every solid black curve with the solid blue curve are fixed points of the Poincaré map, where the condition $z_{n+1} = z_n$ is met.

Analysing Figure 3, it is possible to observe that, for monochromatic inputs, a limit cycle is established. Complementarily, in Figure 4, using the fixed points of the Poincaré maps, the oscillation amplitude is plotted as a function of the f_e amplitude and frequency. As observed in Figure 4 (top), for small values of A, the oscillation amplitude is approximately linear in A. However, as the force amplitude increases, the effect of $g(\boldsymbol{z})$ can be appreciated and the normalised maximum displacement remains below 1. On the other hand, the system response for different frequencies, ω, can be observed in Figure 4 (bottom). Here, it is shown how IGDE (4) acts as a nonlinear low-pass filter for the external force.

Although extrapolating the results from monochromatic to panchromatic excitation force is not trivial, it is possible to observe that, only for $A(t) \to \infty$ and $\omega(t) \to 0$, the amplitude oscillation reaches $|z| = 1$. Hence, assuming (H1)–(H2) hold, it is predicted that constraints cannot be surpassed. Formally, it would be possible to extend the present study to a panchromatic f_e by decomposing f_e in terms of a Fourier series and following (over a moving average window) the analysis presented in [9]. For the time being, however, using the analysis from [9] is beyond the scope of this present paper.

IV. Application Case Study

In this section, in-silico evaluations are conducted on a one-degree-of-freedom point absorber WEC to thoroughly assess the causal constraint mechanism. The simulation parameters are presented in Subsection IV-A. Then, using different excitation force profiles, the efficacy of the constraint method is evaluated in Subsections IV-B and IV-C.

A. WEC model

Consider the one-degree-of-freedom WEC dynamics:

$$\Sigma_w : \begin{cases} \dot{v} = \mathcal{M}\left(-\mathbf{h}\boldsymbol{q} - k_x x + f_e + f_u\right), & \text{(22a)} \\ \dot{x} = v, & \text{(22b)} \\ \dot{\boldsymbol{q}} = \mathbf{F}\boldsymbol{q} + \mathbf{g}v, & \text{(22c)} \\ y = v, & \text{(22d)} \end{cases}$$

where x is displacement, v is velocity, $\boldsymbol{q} \in \mathbb{R}^7$ are the radiation states, and f_e is the wave excitation force, which can be modelled as an external bounded disturbance with zero mean. When applicable, f_e is generated using the Bretschneider spectrum [13], considering a peak period $T_p = 8s$, and significant wave height $H_s = 1m$. Also, $\mathcal{M} = 6.8 \times 10^{-6}$, $k_x = 5.57 \times 10^5$, and $\mathbf{F}$, $\mathbf{g}$, and $\mathbf{h}$ are:

$$\mathbf{F} = \begin{bmatrix} -7 & -24 & -47 & -57 & -43 & -18 & -3.4 \\ 1 & 0 & 0 & 0 & 0 & 0 & 0 \\ 0 & 1 & 0 & 0 & 0 & 0 & 0 \\ 0 & 0 & 1 & 0 & 0 & 0 & 0 \\ 0 & 0 & 0 & 1 & 0 & 0 & 0 \\ 0 & 0 & 0 & 0 & 1 & 0 & 0 \\ 0 & 0 & 0 & 0 & 0 & 1 & 0 \end{bmatrix}, \quad \text{(23a)}$$

$$\mathbf{g} = \begin{bmatrix} 1.46 \cdot 10^5 & 0 & 0 & 0 & 0 & 0 & 0 \end{bmatrix}^\intercal, \quad \text{(23b)}$$

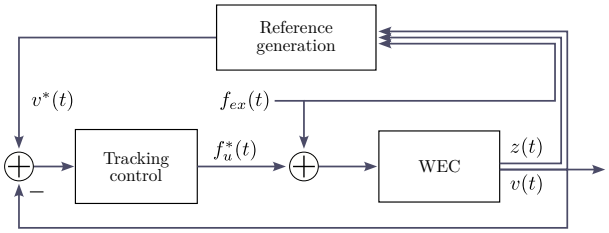

Figure 5. Illustrative diagram of a VT control loop for WECs.

$$\mathbf{h} = \begin{bmatrix} 0.21 & 1.1 & 3.8 & 4.6 & 3 & 0.64 & 0.014 \end{bmatrix} \cdot -10^{-5}. \quad (23c)$$

B. Velocity tracking structure for WECs

The velocity tracking (VT) control structure used in this paper is presented in Figure 5. In essence, the VT structure requires a velocity reference, $v^*(t)$, which is provided by a variation of (4). Specifically:

$$v^* = F(k_0 \cdot f_e, z/z_M, \dot{z}/v_M), \quad (24)$$

with $k_0 = 1 \cdot 10^{-5}$, and z_M being the position constraint:

$$|z| < z_M = 2m, \quad (25)$$

where v_M is determined by the application requirements, and $k_0 \approx 1/\max\{f_e\}$. Complementarily, the VT structure requires a f_e estimator [14] and a tracking control. Due to its inherent robustness, a sliding-mode super-twisting (ST) control is employed [15][16]. Specifically, the ST control law is defined as:

$$f_u = -k_1|v - v^*|^{1/2}\text{sign}(v - v^*) - k_2 \int_{t_0}^{t} \text{sign}(v - v^*)\text{d}\tau, \quad (26)$$

which robustly, and in finite time, achieves

$$\mathcal{S} = \{\boldsymbol{x} \in \mathcal{X} : v - v^* = \sigma(\boldsymbol{x}, t) = \dot{\sigma}(\boldsymbol{x}, t) = 0\}. \quad (27)$$

Hence, robust tracking of the velocity reference is guaranteed and the reduced-order closed-loop dynamics result:

$$\Sigma_w : \begin{cases} \dot{z} = k_0 \left(\dfrac{e^{1-\alpha(z/z_M, \dot{z}/v_M)} - 1}{e^1 - 1} \right) \cdot \hat{f}_e, & (28a) \\ \dot{\boldsymbol{q}} = \mathbf{F}\boldsymbol{q} + \mathbf{g}\dot{z}, & (28b) \\ y = \dot{z}. & (28c) \end{cases}$$

Since $\mathbf{F}$ is Hurwitz, the zero dynamics of (28) are stable. Also, $\dot{z}$ and z are constrained to the ellipse defined by $\alpha(z/z_M, \dot{z}/v_M) = 1$.

C. Constraint mechanism performace evaluation

To evaluate the performance of the constraint mechanism, time-domain simulations are conducted. First, results using a monochromatic excitation force are presented in Subsection IV-C.1. Then, the performance of the constraint method using a non-monochromatic excitation force is preliminarily evaluated in Subsection IV-C.2. Recall that the evaluation in terms of power absorption is presented in [8], where it is shown that the proposed constraint mechanism exhibits close-to-optimal performance.

1) Monochromatic excitation force results: Let the excitation force be defined as $f_e = 2 \cdot 10^5 \sin(0.78t)$, and evaluate three cases with $v_M \in [2.3, 1.5, 0.7]m/s$. The v vs z phase plane with initial conditions $z_0 = v_0 = 0$ are presented in Figure 6. Here, it is possible to assess that (i) every trajectory remains in $\mathcal{R}_c$, (ii) a limit cycle is established, and (iii) using a larger v_M, the position excursion is larger. This implies that v_M may be employed as a tuning parameter, since in wave energy systems, v_M is generally a flexible parameter.

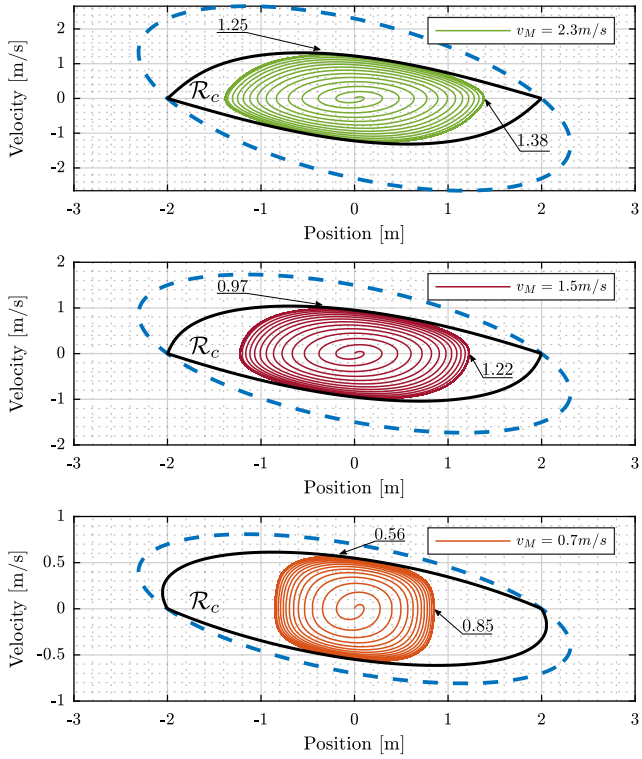

Figure 6. Phase plane v vs z. Three separate cases, with $v_M \in [2.3, 1.5, 0.7]$, are presented.

2) Non-monochromatic excitation force results: Extending the results from monochromatic to polychromatic excitation force is not trivial. However, to evaluate the performance of the constraint method, three different cases considering $v_M \in [2.3, 1.5, 0.7]m/s$ with a polychromatic f_e are analysed. First, the evolution of the system states, position and velocity is presented in the time domain in Figure 7. It can be observed that, using ST control, the constraint requirements are satisfied and the WEC operates within the specified limits. To analyse satisfaction of constraints for longer periods, 2000s simulations are conducted. Then, the phase plane v vs z for the cases $v_M \in [2.3, 1.5, 0.7]$ is presented in Figure 8, where it can be appreciated that the trajectories remain within $\mathcal{R}_c$. The phase plane in Figure 8 is also an effective method to visualise the distribution of the trajectories for a panchromatic function. In the cases with $v_M = 2.3m/s$ and $v_M = 1.5m/s$, the trajectories concentrate at the edges of the ellipse, implying that the constraint mechanism actively reduces both position and velocity values to keep the system in $\mathcal{R}_c$, by making $F(\cdot) \to 0$. However, with $v_M = 0.7m/s$,

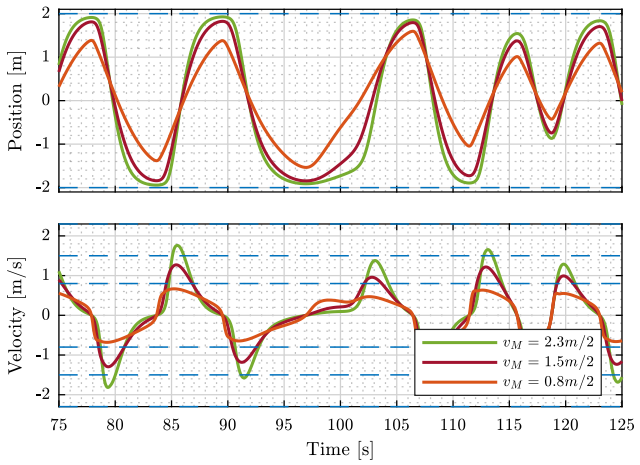

Figure 7. Time evolution of position and velocity. Three separate cases, with $v_M \in [2.3,\ 1.5,\ 0.7]$, are presented.

the position is penalised, and z is further away from the limit z_M. As in the monochromatic case, it is concluded that v_M may be employed as a tuning parameter.

V. Conclusions

This paper presents a preliminary stability analysis of *Symphony* position *and* velocity constraint mechanism. The proposed method is a novel and simple approach for handling hard position *and* velocity constraints in wave energy systems, and, importantly, it can also be used as a complement for other !OB controllers. The proposed method operates using a velocity tracking structure and, to ensure compliance with system constraints, uses an IGDE as a velocity reference generator. Among the advantages of the method are simplicity of implementation and use, robustness to satisfy constraints, and, as detailed in [8], close-to-optimal performance in terms of power absorption. Additionally, a key feature of the proposed constraint method is that it does not rely on complex tuning or optimisation routines to ensure system performance and safety. Hence, the proposed algorithm could serve as an essential complement for real-time implementation of !OB control strategies.

Future work includes (i) a formal analysis of the stability for poly/panchromatic excitation forces and (ii) an assessment of the constraint method performance considering noisy environments and faulty measurements, and a variety of tracking controllers.

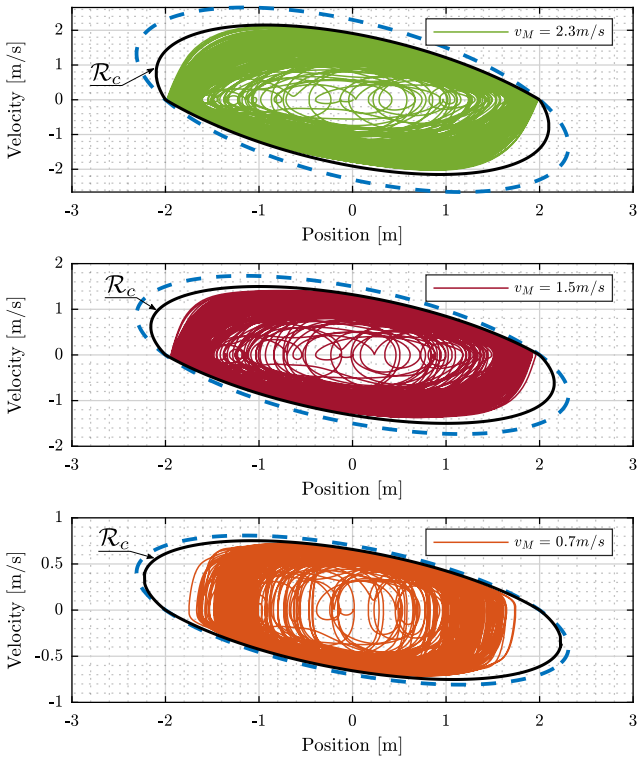

Figure 8. Phase plane v vs z. Three separate cases, with $v_M \in [2.3,\ 1.5,\ 0.7]$, are presented.

References

[1] N. Faedo, G. Mattiazzo, and J. V. Ringwood, "Robust energy-maximising control of wave energy systems under input uncertainty," in *2022 European Control Conference (ECC)*. IEEE, 2022, pp. 614–619.

[2] A. Garcia-Teruel and D. Forehand, "Optimal wave energy converter geometry for different modes of motion," in *Advances in Renewable Energies Offshore*, 2018, pp. 299–307.

[3] G. Bacelli and J. V. Ringwood, "Numerical optimal control of wave energy converters," *IEEE Transactions on Sustainable Energy*, vol. 6, no. 2, pp. 294–302, 2014.

[4] D. García-Violini, N. Faedo, F. Jaramillo-Lopez, and J. V. Ringwood, "Simple controllers for wave energy devices compared," *Journal of Marine Science and Engineering*, vol. 8, no. 10, p. 793, 2020.

[5] X. Huang, Z. Lin, and X. Xiao, "Simple and low-model-dependent strategy for the economic and safe control of direct-drive wave energy converters," *IEEE Transactions on Energy Conversion*, vol. 38, no. 4, pp. 2263–2272, Dec. 2023.

[6] N. Faedo, F. Carapellese, G. Papini, E. Pasta, F. D. Mosquera, F. Ferri, and T. K. A. Brekken, "An anti-windup mechanism for state constrained linear control of wave energy conversion systems: Design, synthesis, and experimental assessment," *IEEE Transactions on Sustainable Energy*, vol. 15, no. 2, pp. 964–973, Apr. 2024.

[7] Y. Lao, J. T. Scruggs, A. Karthikeyan, and M. Previsic, "Discrete-time causal control of a wave energy converter with finite stroke in stochastic waves," *IEEE Transactions on Control Systems Technology*, vol. 30, no. 3, pp. 1198–1214, May 2022.

[8] P. Fornaro, Z. Lin, E. Gelos, and J. V. Ringwood, "Symphony: The ultimate wave energy controller?" in *EWTEC European wave and tidal energy Conference, Madeira, Portugal*, Sep. 2025.

[9] C. Kaas-Petersen, "Computation of quasi-periodic solutions of forced dissipative systems," *Journal of Computational Physics*, vol. 58, no. 3, pp. 395–408, May 1985.

[10] W. Cummins, "The impulse response function and ship motions," *Schiffstechnik*, vol. 9, pp. 101—-109, 1962.

[11] N. Faedo, S. Olaya, and J. V. Ringwood, "Optimal control, MPC and MPC-like algorithms for wave energy systems: An overview," *IFAC J. Syst. Control*, vol. 1, pp. 37–56, Sep. 2017.

[12] A. Mérigaud and J. V. Ringwood, "Free-surface time-series generation for wave energy applications," *IEEE Journal of Oceanic Engineering*, vol. 43, no. 1, pp. 19–35, 2018.

[13] C. L. Bretschneider, *Wave variability and wave spectra for wind-generated gravity waves*. USA: The Board, 1959, no. 118.

[14] P. Fornaro, F. D. Mosquera, P. F. Puleston, C. A. Evangelista, and J. V. Ringwood, "Homogeneous filtering unknown input observer for wave energy applications," in *63rd IEEE Conference on Decision and Control*, Milan, Italy, Dec. 2024.

[15] A. Levant, "Sliding order and sliding accuracy in sliding mode control," *International Journal of Control*, vol. 58, no. 6, pp. 1247–1263, Dec. 1993.

[16] A. Levant, "Higher-order sliding modes, differentiation and output-feedback control," *Int. J. Control*, vol. 76, no. 9-10, jan 2003.